Polymer 49 (2008) 3938–3949

Contents lists available at ScienceDirect

Polymer

journal homepage: www.elsevier.com/locate/polymer

Synthesis and characterization of optically active liquid crystalline polyacrylates containing mesogenic phenylbenzoate groups

Jui-Hsiang Liu*, Yu-Kan Wang, Chien-Chih Chen, Po-Chih Yang, Feng-Ming Hsieh, Yi-Hong Chiu

Department of Chemical Engineering, National Cheng Kung University, No. 1 University Road, Tainan 70101, Taiwan, ROC

ARTICLE INFO

Article history:
Received 11 May 2008
Received in revised form 27 June 2008
Accepted 3 July 2008
Available online 15 July 2008

Keywords:
Liquid crystals
Polymerization
Chiral

ABSTRACT

A series of novel side chain liquid crystalline polyacrylates with pendant chiral groups were synthesized. It was found that monomers with electron releasing $-OC_4H_9$ terminal groups seem beneficial for the formation of liquid crystalline phases. Copolymerization of the monomers was carried out and the physical properties of the copolymers were investigated. All synthesized polymers revealed liquid crystalline phases and appeared highly thermally stable with decomposition temperatures (T_d) at 10% weight loss greater than 384 °C and about 50% weight loss occurred beyond 442 °C under nitrogen atmosphere. Two miscible chiral compounds were also synthesized and used as chiral dopants to induce cholesteric liquid crystalline phases of polymers. Liquid crystalline phases of the polymers were investigated using DSC and XRD, and confirmed with POM technique. The optical properties of the induced cholesteric liquid crystalline polymers were investigated using UV–vis spectrometer. The appearance and the color variation of the polymer films before and after UV irradiation were also investigated. Typical helical morphology of the cholesteric liquid crystalline film was analyzed by SEM technique.

1. Introduction

Systematic investigations of the synthesis, characterization and applications of side chain liquid crystalline polymers (SCLCPs) began only after Ringsdorf [1] and others proposed that a flexible spacer should be inserted between the polymeric main chain and the mesogenic side groups to decouple the motions of the main chain and side groups in the liquid crystalline state. Since, Ringsdorf et al. developed the first side chain liquid crystal polymer in 1978; research in polymer liquid crystalline science and its technological applications have dramatically increased [2–6]. The macromolecular structure of SCLCPs depends on both the composition of the polymer main chain and the side chain with liquid crystalline character. Therefore, the design and synthesis of SCLCPs can be surely fulfilled via the selection of different polymer main chains and side chains according to practical applications.

In recent years, there have been many publications devoted to the studies of the preparation and the applications of photosensitive liquid crystalline polymer composed of chiral moiety [7–10]. The working principle of photocontrollable cholesteric polymers introduced photosensitive or photoisomerized mesogenic fragments such as azobenzene and stilbene which could reverse their configuration when irradiated with different light wavelengths. When the configuration changed, the twisting power or optical characteristics changed at the same time. Composite films were photoirradiated at different wavelengths to bring about the photoisomerization of the guest azobenzene. Azobenzene is an attractive photosensitive material because of its simple photochemistry and ease of chemical modification. Azobenzene dissolved in a chiral nematic (cholesteric) liquid crystal provides photocontrollability of the helical pitches as a result of *E–Z* photoisomerization, as demonstrated by Sackmann [11]. On the other hand, a chiral azobenzene derivative dissolved in a nematic liquid crystal can act as a chiral dopant to induce a chiral nematic phase and a phototrigger to control the generated helical pitch [12–14].

In a series of studies, chiral monomers and chiral dopants were synthesized and their uses in the induction of cholesteric liquid crystal phases were also studied [15–21]. In the studies, the photochromic function was designed with azobenzene derivatives. In order to improve the thermal stability of liquid crystalline polymers without phase separation, a series of liquid crystalline polyacrylates with mesogenic phenylbenzoate groups and two miscible chiral dopants were synthesized. Their mesomorphic properties and thermal stability were evaluated with DSC, POM, X-ray, and TGA. Another advantageous embodiment of the method according to this investigation is characterized in that the convertible compound comprises of a photoisomerizable chiral compound. The different isomeric forms of such an isomerizable chiral compound usually have a different influence on the pitch of the molecular helix of the cholesterically ordered material. By locally changing the ratio of

* Corresponding author. Tel.: +886 6 2757575; fax: +886 6 2384590.
E-mail address: jhliu@mail.ncku.edu.tw (J.-H. Liu).

0032-3861/$ – see front matter © 2008 Elsevier Ltd. All rights reserved.
doi:10.1016/j.polymer.2008.07.009

these isomeric forms by way of irradiation, the pitch is changed. This provides an elegant possibility of manufacturing patterned layers of a polymer material with a cholesteric ordering and a different pitch.

2. Experimental

2.1. Materials

ZLI-2293 and E7, two commercially available eutectic mixtures of several low molecular weight nematic liquid crystals, were purchased from Merck (Darmstadt, Germany) and were used as host liquid crystals without further purification. 4-Hydroxybenzoic acid (99.0%), 6-chloro-1-hexanol (95.0%), 11-bromo-1-undecanol (97.0%), acryloyl chloride (98.0%), 4-butoxyphenol (99.0%), 4-cyanophenol (99.0%), L(−)-menthol (99.7%), cholesterol (95.0%), *p*-cinnamic acid (98.0%), *N*,*N*′-dicyclohexylcarbodiimide (DCC; 99.0%), and 2,2′-azobisisobutyronitrile (AIBN; 98.0%) were purchased from Acros Chemical Co. 4-Dimethylaminopyridine (DMAP; 99.0%) was purchased from Lancaster Chemical Co. All organic solvents were purchased from Aldrich Chemical Co. Dichloromethane (CH_2Cl_2) was distilled over calcium hydride under argon immediately before use, and other solvents were used without any further purification. Analytical thin-layer chromatography was conducted on Merck aluminum plates with 0.2 mm of silica gel 60F-254. Anhydrous sodium sulfate was used to dry all organic extracts. AIBN was freshly recrystallized from methanol.

2.2. Measurements

All new compounds were identified by ^{1}H NMR spectra, FTIR spectra, and elemental analysis (EA). FTIR spectra were recorded as a KBr disk on a Jasco VALOR III (Tokyo, Japan) FTIR spectrophotometer. Nuclear magnetic resonance (NMR) spectra were obtained on a Bruker ^{1}H NMR (400 MHz) and ^{13}C NMR (100.6 MHz) spectra were obtained on a Bruker AMX-400 (Darmstadt, Germany) high-resolution NMR spectrometer, and chemical shifts were reported in ppm with tetramethylsilane (TMS) as an internal standard. Optical rotations were measured at 30 °C in $CHCl_3$ using a Jasco DIP-370 polarimeter with the D-line of sodium ($\lambda = 589$ nm) with a precision of ±0.001°. The measurements were performed using 1% solutions of substances in $CHCl_3$. Elemental analyses were conducted with a Heraeus CHN–O (Darmstadt, Germany) rapid elemental analyzer. Gel permeation chromatography (GPC) measurements were carried out at 40 °C on a Hitachi L-4200 (Osaka, Japan) instrument equipped with TSK gel GMH and G2000H columns using $CHCl_3$ as an eluent and the rate of elution was 1.0 ml min^{-1}; the instrument was calibrated with a polystyrene standard. Differential scanning calorimeter (DSC) was conducted with a Perkin Elmer DSC 7 at a heating and cooling rate of 10 K min^{-1} in a nitrogen atmosphere. The phase transitions were investigated by an Olympus BH-2 polarized light microscope (POM) equipped with Mettler hot stage FP-82 and the temperature scanning rate was determined at a rate 10 K min^{-1}. Thermal decomposition temperature data were recorded under nitrogen atmosphere at a heating rate of 40 K min^{-1} with a thermogravimetric analyzer (TGA) Perkin Elmer TGA 7. UV spectroscopy measurements were carried out with a Jasco V-550 UV–vis spectrophotometer. The X-ray diffraction data were recorded on a Rigaku RINT 2500 series instrument with Ni-filtered Cu Kα radiation. The sample in a quartz capillary was held in a temperature-controlled cell (Rigaku LC high-temperature controller). Scanning electron microscope (SEM) microphotographs were measured with a JEOL HR-FESEM JSM-6700F (Osaka, Japan) instrument. UV light (300 nm; Model UVG-54) with an intensity of 0.6 mW was used as a pumping light to induce photoisomerization of chiral monomers with C=C bonds in $CHCl_3$ solutions. Selective light reflection of the samples was recorded using a USB-2000 fiber optic spectrometer from a Halogen lamp LS-1 as light source.

2.3. Synthesis of monomers and chiral dopants (Schemes 1 and 2)

Synthetic routes for the target monomers and chiral dopants are shown in Schemes 1 and 2, respectively. The following monomers and chiral dopants were synthesized according to the similar procedures described in our previous reports [15,17–21] and the literature [22]. 4-(6-Acryloyloxyhexyloxy) benzoic acid and 4-(6-acryloyloxy-undecyloxy) benzoic acid were synthesized following the processes reported in the literature [22]. (−)-Cholesteryl 4-hydroxybenzoate and (−)-menthyl 4-hydroxybenzoate were synthesized following the processes reported in our previous reports [17,20,21]. The obtained products were purified and then identified using FTIR, ^{1}H NMR, ^{13}C NMR and elemental analysis.

2.3.1. 4-Cyanophenyl-4′-(6-acryloyloxyhexyloxy) benzoate (**1**) (**M1**)

4-(6-Acryloyloxyhexyloxy) benzoic acid (2.92 g, 10.0 mmol), 4-cyanophenol (1.78 g, 15.0 mmol), and 50 ml dry dichloromethane were added to a two-necked glass reactor. *N*,*N*′-Dicyclohexylcarbodiimide (DCC) (3.09 g, 15.0 mmol) and 4-dimethylaminopyridine (DMAP) (0.12 g, 1 mmol) were dissolved in dichloromethane (30 ml), and then added to the solution under nitrogen atmosphere. The reaction mixture was stirred for 24 h at 30 °C. A solid, *N*,*N*′-dicyclohexyl urea, was precipitated and filtered off. The resulting solution was washed with water, dried with anhydrous $MgSO_4$, and evaporated to dryness. The crude product was purified by column chromatography (silica gel, ethyl acetate/hexane = 1/5).

Yield: 45.8%. $T_m = 78.0$ °C. FTIR (KBr, ν_{max}/cm^{-1}): 2940, 2863 (CH_2), 2230 (CN), 1712 (C=O), 1610, 1505 (C–C in Ar), 1196, 1230 (C–O–C), 1630 (C=C). ^{1}H NMR ($CDCl_3$, δ in ppm): 1.47–2.10 (m, 8H, CH_2), 4.04–4.20 (t, 4H, OCH_2), 5.82 (dd, 1H, CH_2=CH), 6.13 (dd, 1H, CH_2=CH), 6.41 (dd, 1H, CH_2=CH), 6.96–6.99 (d, 2H, Ar–H), 7.26–7.37 (d, 2H, Ar–H), 7.72–7.74 (d, 2H, Ar–H), 8.11–8.13 (d, 2H, Ar–H). ^{13}C NMR (100.6 MHz, $CDCl_3$): 24.81, 25.69, 28.78, 29.23 (CH_2); 63.00, 68.17 (OCH_2); 118.27 (CN); 113.15, 122.77, 129.53, 133.74 (aromatic); 128.81 131.86 (C=C); 109.60, 120.58, 153.65, 159.72 (aromatic quaternary); 165.89, 166.32 (C=O). Anal: calcd for $C_{23}H_{23}NO_5$, C 70.23, H 5.85, N 3.56; found C 70.18, H 5.80, N 3.61%.

2.3.2. 4-Cyanophenyl-4′-(6-acryloyloxyundecyloxy) benzoate (**2**) (**M2**)

The synthesized procedure of **M2**–**M6** and chiral dopants **7** and **8** was analogous to **M1**.

Yield: 52.3%. $T_m = 85.2$ °C. FTIR (KBr, ν_{max}/cm^{-1}): 2930, 2865 (CH_2), 2229 (CN), 1715 (C=O), 1611, 1506 (C–C in Ar), 1198, 1231 (C–O–C), 1632 (C=C). ^{1}H NMR ($CDCl_3$, δ in ppm): 1.37–1.88 (m, 18H, CH_2), 4.10–4.15 (t, 4H, OCH_2), 5.85 (dd, 1H, CH_2=CH), 6.14 (dd, 1H, CH_2=CH), 6.33 (dd, 1H, CH_2=CH), 7.10–7.12 (d, 2H, Ar–H), 7.51–7.53 (d, 2H, Ar–H), 7.89–7.91 (d, 2H, Ar–H), 8.11–8.13 (d, 2H, Ar–H). ^{13}C NMR (100.6 MHz, $CDCl_3$): 25.98, 28.37, 28.49, 28.57, 29.13, 29.03, 29.19 (CH_2); 62.99, 68.20 (OCH_2); 118.26 (CN); 113.16, 122.77, 129.53, 133.73 (aromatic); 128.80 131.85, (C=C); 109.60, 120.57, 153.63, 159.71 (aromatic quaternary); 165.90, 166.31 (C=O). Anal: calcd for $C_{28}H_{33}NO_5$, C 72.57, H 7.13, N 3.02; found C 72.52, H 7.06, N 3.05%.

2.3.3. 4-Butoxyphenyl-4′-(6-acryloyloxyhexyloxy) benzoate (**3**) (**M3**)

Yield: 58.4%. K 33.3 °C N 57.1 °C I (cooling). FTIR (KBr, ν_{max}/cm^{-1}): 2933, 2854 (CH_2), 1730 (C=O), 1604, 1509 (C–C in Ar), 1245, 1194 (C–O–C), 1627 (C=C). ^{1}H NMR ($CDCl_3$, δ in ppm): 0.94–0.98 (t, 3H, CH_3), 1.47–1.52 (m, 12H, CH_2), 3.99–4.33 (t, 6H, OCH_2), 5.85 (dd, 1H, CH_2=CH), 6.15 (dd, 1H, CH_2=CH), 6.21 (dd, 1H, CH_2=CH),

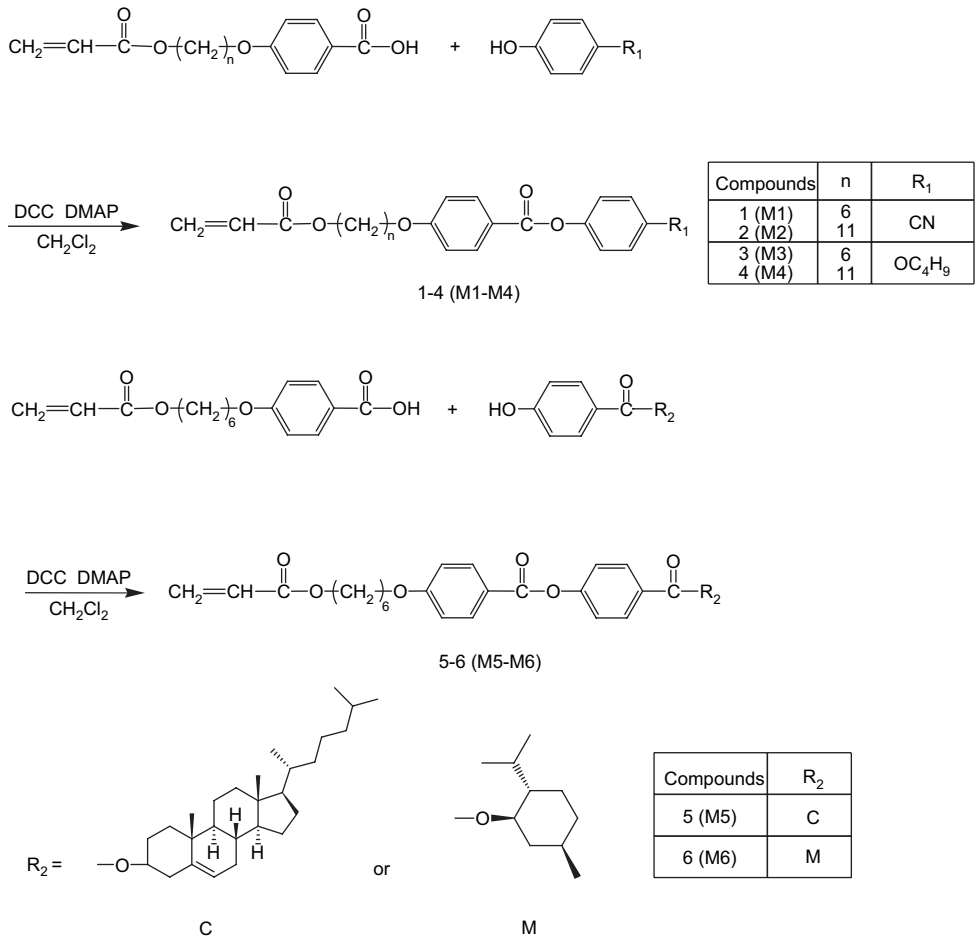

Compounds	n	R_1
1 (M1)	6	CN
2 (M2)	11	
3 (M3)	6	OC_4H_9
4 (M4)	11	

Compounds	R_2
5 (M5)	C
6 (M6)	M

Scheme 1. Synthetic routes of monomers **M1**–**M6**.

6.96–6.99 (d, 2H, Ar–H), 7.07–7.15 (d, 4H, Ar–H), 8.07–8.11 (d, 2H, Ar–H). ^{13}C NMR (100.6 MHz, $CDCl_3$): 13.85 (CH_3); 19.24, 24.81, 25.70, 28.78, 29.23, 31.32 (CH_2); 62.99, 68.06, 68.17 (OCH_2); 113.14, 114.05, 122.45, 129.53 (aromatic); 128.81 131.86, (C═C); 120.57, 143.17, 156.92, 159.73 (aromatic quaternary); 165.88, 166.31 (C═O). Anal: calcd for $C_{26}H_{32}O_6$, C 70.91, H 7.27; found C 70.84, H 7.31%.

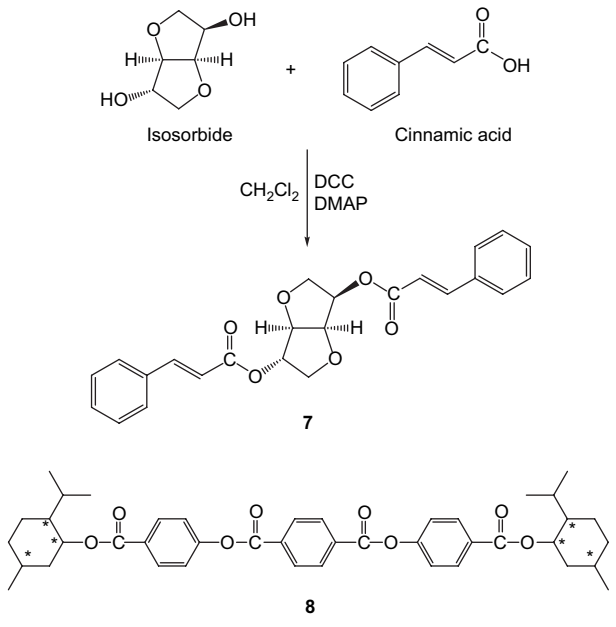

Scheme 2. Synthetic routes of chiral dopants **7** and **8**.

2.3.4. 4-Butoxyphenyl-4′-(6-acryloyloxyundecyloxy) benzoate (***4***) (***M4***)

Yield: 62.1%. K 60.7 °C S_A 63.3 °C N 64.3 °C I. FTIR (KBr, ν_{max}/cm^{-1}): 2928, 2853 (CH_2), 1725 (C═O), 1601, 1509 (C–C in Ar), 1248, 1195 (C–O–C), 1634 (C═C). ^{1}H NMR ($CDCl_3$, δ in ppm): 0.95–0.98 (t, 3H, CH_3), 1.47–1.83 (m, 22H, CH_2), 3.77–4.27 (t, 6H, OCH_2), 5.85 (dd, 1H, CH_2═CH), 6.13 (dd, 1H, CH_2═CH), 6.35 (dd, 1H, CH_2═CH), 6.95–6.99 (d, 2H, Ar–H), 7.06–7.15 (d, 4H, Ar–H), 8.08–8.10 (d, 2H, Ar–H). ^{13}C NMR (100.6 MHz, $CDCl_3$): 13.84 (CH_3); 19.23, 25.98, 28.38, 28.51, 28.57, 29.03, 29.19, 29.51, 31.31 (CH_2); 62.99, 68.08, 68.20 (OCH_2); 113.15, 114.06, 122.46, 129.53 (aromatic); 128.80 131.85, (C═C); 120.57, 143.16, 156.91, 159.72 (aromatic quaternary); 165.89, 166.31 (C═O). Anal: calcd for $C_{31}H_{42}O_6$, C 72.94, H 8.24; found C 72.81, H 8.20%.

2.3.5. (−)-4-Cholesteryl 4-(6-acryloyloxyhexyloxy) phenyl-4′-benzoate (***5***) (***M5***)

Yield: 45.6%. K 130.2 °C N* 205.4 °C I. $[\alpha]_D = -12.5°$. FTIR (KBr, ν_{max}/cm^{-1}): 2936, 2852 (CH_2), 1699 (C═O in Ar–COO–), 1636, 1510 (C–C in Ar), 1200, 1232 (C–O–C), 1636 (C═C). ^{1}H NMR ($CDCl_3$, δ in ppm): 0.79–1.19 (m, 15H, CH_3), 1.26–2.60 (m, 36H, CH_2), 4.13–4.17 (t, 4H, CH_2O), 4.77–4.82 (s, 1H, Ar–COOCH), 5.45 (s, 1H, CH═C), 5.84 (dd, 1H, CH_2═CH), 6.15 (dd, 1H, CH_2═CH), 6.35 (dd, 1H, CH_2═CH), 7.04–7.10 (d, 2H, Ar–H), 7.34–7.42 (d, 2H, Ar–H), 8.10–8.13 (d, 4H, Ar–H). ^{13}C NMR (100.6 MHz, $CDCl_3$): 12.01, 18.91, 19.30, 22.51 (CH_3); 21.31, 24.30, 24.81, 25.70, 28.77, 29.22, 32.21, 32.50, 36.71, 38.40,

39.81, 40.01 (CH_2); 62.99, 68.16 (OCH_2); 28.21, 31.81, 36.10, 50.39, 56.59, 57.01, 75.11, 122.61, 139.91 (CH); 113.14, 121.24, 128.81, 129.51 (aromatic); 128.81 131.85, (C=C); 120.55, 125.66, 152.25, 159.71 (aromatic quaternary); 165.87, 166.29, 166.76 (C=O). Anal: calcd for $C_{50}H_{68}O_7$, C 76.82, H 8.71; found C 76.74, H 8.64%.

*2.3.6. (−)-4-Menthyl 4-(6-acryloyloxyhexyloxy) phenyl-4′-benzoate (**6**) (**M6**)*

Yield: 42.0%. $T_m = 32.6$ °C. $[\alpha]_D = -46.2°$. FTIR (KBr, ν_{max}/cm^{-1}): 2934, 2870 (CH_2), 1712 (C=O in Ar–COO–), 1610, 1505 (C–C in Ar), 1196, 1230 (C–O–C), 1630 (C=C). ^{1}H NMR ($CDCl_3$, δ in ppm): 0.77–0.94 (m, 9H, CH_3), 1.09–2.11 (m, 17H, CH_2), 4.00–4.07 (t, 2H, CH_2OPh), 4.16–4.20 (t, 2H, $COOCH_2$), 4.90–4.97 (m, 1H, $OCHCH_2$), 5.80–5.83 (dd, 1H, CH_2=CH), 6.09–6.16 (dd, 1H, CH_2=CH), 6.38–6.43 (dd, 1H, CH_2=CH), 6.96–6.99 (d, 2H, Ar–H), 7.26–7.29 (d, 2H, Ar–H), 8.10–8.16 (d, 4H, Ar–H). ^{13}C NMR (100.6 MHz, $CDCl_3$): 21.06, 22.03 (CH_3); 23.17, 25.70, 28.77, 34.22, 39.05, 62.99, 68.16 (CH_2); 62.99, 68.17 (OCH_2); 24.68, 29.70, 48.31, 75.44 (CH); 113.15, 121.23, 128.15, 129.52 (aromatic); 128.80, 131.85, (C=C); 120.56, 125.17, 152.26, 159.71 (aromatic quaternary); 165.88, 166.30, 167.31 (C=O). Anal: calcd for $C_{33}H_{42}O_7$, C 72.00, H 7.64; found C 72.04, H 7.81%.

*2.3.7. (−)-Isosorbide 2,5-bis(cinnamate) (**7**)*

Yield: 38.5%. $T_m = 116.3$ °C. $[\alpha]_D = -65.0°$. FTIR (KBr, cm^{-1}): 2980, 2861 (CH_2), 1730 (C=O), 1604, 1503 (C–C in Ar), 1640 (C=C). ^{1}H NMR ($CDCl_3$, δ in ppm): 3.88–4.05 (m, 4H, CH_2O), 4.57 (m, 1H, CH), 4.95 (m, 1H, CH), 5.26–5.33 (dd, 2H, CH=CH), 6.53–6.63 (dd, 2H, CH=CH), 7.43–7.75 (m, 10H, Ar–H). ^{13}C NMR (100.6 MHz, $CDCl_3$): 68.67 (CH_2); 73.73 74.92, 79.78, 79.89 (CH); 129.29, 129.97, 131.50 (aromatic); 119.48 146.69, (C=C); 135.7 (aromatic quaternary); 168.330, 169.92 (C=O). Anal: calcd for $C_{24}H_{22}O_6$, C 70.93, H 5.46; found C 71.18, H 5.67%.

*2.3.8. (−)-Bis-[4-(menthyloxycarbonyl)phenyl] terephthalate (**8**)*

Yield: 37.9%. $T_m = 141.8$ °C. $[\alpha]_D = -64.2°$. FTIR (KBr, cm^{-1}): 2951, 2875 (CH_2), 1690 (C=O), 1604, 1503 (C–C in Ar). ^{1}H NMR ($CDCl_3$, δ in ppm): 0.80–0.98 (m, 18H, CH_3), 1.07–2.15 (m, 18H, CH_2), 4.92–4.98 (m, 2H, CH), 7.32–7.34 (d, 4H, Ar–H), 8.14–8.16 (d, 4H, Ar–H), 8.35 (d, 4H, Ar–H). ^{13}C NMR (100.6 MHz, $CDCl_3$): 21.05, 22.02 (CH_3); 23.17, 34.21, 39.04 (CH_2); 24.68, 29.70, 48.31, 75.43 (CH); 121.22, 128.14, 128.98 (aromatic); 125.16, 129.84, 152.27 (aromatic quaternary); 165.87, 167.31 (C=O). Anal: calcd for $C_{42}H_{50}O_8$, C 73.90, H 7.33; found C 73.85, H 7.36%.

2.4. Synthesis of polymers (Scheme 3)

Homopolymers and copolymers were obtained by the polymerization of monomers in benzene in presence of 3 mol% of 2,2′-azobisisobutyronitrile (AIBN) at 60 °C for 24 h. The feed molar ratio of 83/17 of the comonomers was used to prepare binary copolymers. The general synthetic procedures for the polymers are described as follows: a solution of predetermined amount of monomers in benzene with 3 mol% of 2,2′-azobisisobutyronitrile (AIBN) were poured into a glass polymerization tube equipped with a sealing cap, which was degassed in a vacuum by using a freeze-thaw technique, and then sealed. After completion of polymerization, the polymers were precipitated in a large amount of methanol solution, and then the crude polymers were purified by dissolving them in benzene and reprecipitated in methanol, and then dried in a vacuum.

*2.4.1. **P1***

M1 (0.2 g, 0.509 mmol), AIBN (2.5 mg, 0.0153 mmol), and benzene (2 ml) were used. Yield: 78.0%. FTIR (KBr, ν_{max}/cm^{-1}): 2945, 2867 (CH_2), 2231 (CN), 1735 (C=O in Ar–COO–), 1610, 1512 (C–C in Ar), 1255, 1199 (C–O–C). ^{1}H NMR ($CDCl_3$, δ in ppm): 1.19–2.03 (m, 11H, CH_2), 3.92–3.94 (m, 4H, CH_2O), 6.84 (m, 2H, Ar–H), 7.19 (m, 2H, Ar–H), 7.61 (m, 2H, Ar–H), 7.98 (m, 2H, Ar–H). Anal: calcd for feed, C 70.23, H 5.85, N 3.56; found C 70.85, H 5.56, N 3.52%.

*2.4.2. **P2***

P2 was prepared by a procedure similar to that for **P1**, using **M2** instead of **M1**. Yield: 69.5%. FTIR (KBr, ν_{max}/cm^{-1}): 2941, 2862 (CH_2), 2229 (CN), 1732 (C=O in Ar–COO–), 1608, 1505 (C–C in Ar), 1253, 1202 (C–O–C). ^{1}H NMR ($CDCl_3$, δ in ppm): 1.29–2.25 (m, 21H, CH_2), 3.99 (m, 4H, CH_2O), 6.92 (m, 2H, Ar–H), 7.30 (m, 2H, Ar–H), 7.68 (m,

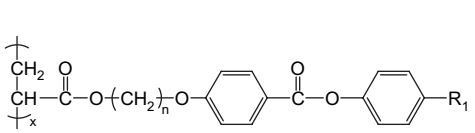

Polymer	n	R_1
P1	6	CN
P2	11	
P3	6	OC_4H_9
P4	11	

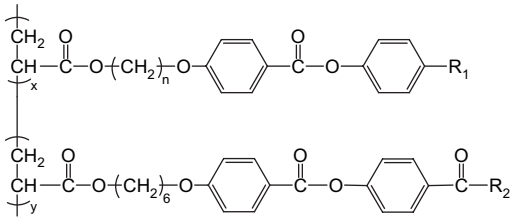

Copolymer	n	R_1	R_2
CP1	6	CN	C
CP2	11		
CP3	6	CN	M
CP4	11		
CP5	6	OC_4H_9	C
CP6	11		
CP7	6	OC_4H_9	M
CP8	11		

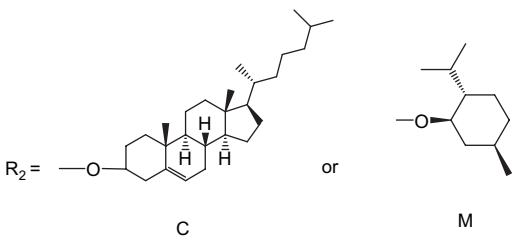

Scheme 3. Chemical structures of homopolymers **P1**–**P4** and copolymers **CP1**–**CP8**.

2H, Ar–H), 8.07 (m, 2H, Ar–H). Anal: calcd for feed, C 72.57, H 7.13, N 3.02; found C 72.85, H 7.18, N 3.06%.

2.4.3. *P3*

P3 was prepared by a procedure similar to that for **P1**, using **M3** instead of **M1**. Yield: 76.0%. FTIR (KBr, ν_{max}/cm^{-1}): 2940, 2863 (CH_2), 1730 (C=O in Ar–COO–), 1606, 1509 (C–C in Ar), 1252, 1197 (C–O–C). ^1H NMR ($CDCl_3$, δ in ppm): 0.97 (m, 3H, CH_3), 1.26–2.28 (m, 15H, CH_2), 3.94 (m, 6H, CH_2O), 6.88 (m, 4H, Ar–H), 7.05 (m, 2H, Ar–H), 8.07 (m, 2H, Ar–H). Anal: calcd for feed, C 70.91, H 7.27; found C 71.34, H 7.05%.

2.4.4. *P4*

P4 was prepared by a procedure similar to that for **P1**, using **M4** instead of **M1**. Yield: 75.1%. FTIR (KBr, ν_{max}/cm^{-1}): 2934, 2856 (CH_2), 1726 (C=O in Ar–COO–), 1613, 1516 (C–C in Ar), 1256, 1203 (C–O–C). ^1H NMR ($CDCl_3$, δ in ppm): 0.96 (m, 3H, CH_3), 1.12–2.27 (m, 25H, CH_2), 3.95 (m, 6H, CH_2O), 6.90 (m, 4H, Ar–H), 7.07 (m, 2H, Ar–H), 8.08 (m, 2H, Ar–H). Anal: calcd for feed, C 72.94, H 8.24; found C 72.35, H 8.38%.

2.4.5. *CP1*

M1 (142.2 mg, 0.340 mmol), **M5** (57.8 mg, 0.074 mmol), AIBN (2.14 mg, 0.0131 mmol), and benzene (2 ml) were used. Yield: 57.2%. FTIR (KBr, ν_{max}/cm^{-1}): 2940, 2862 (CH_2), 2230 (CN), 1728 (C=O in Ar–COO–), 1607, 1508 (C–C in Ar), 1255, 1199 (C–O–C). ^1H NMR ($CDCl_3$, δ in ppm): 0.85–0.91 (m, CH_3), 1.10–2.43 (m, CH_2), 3.96 (m, OCH_2), 4.83 (m, COOCH), 5.40 (m, C=CH), 6.89 (m, Ar–H), 7.25 (m, Ar–H), 7.64 (m, Ar–H), 8.04 (m, Ar–H). Anal: calcd for $C_{73}H_{91}NO_{12}$, C 74.68, H 7.76, N 1.19; found C 73.12, H 7.09, N 1.63%.

2.4.6. *CP2*

CP2 was prepared by a procedure similar to that for **CP1**, using **M2** instead of **M1**. Yield: 62.4%. FTIR (KBr, ν_{max}/cm^{-1}): 2936, 2870 (CH_2), 2228 (CN), 1717 (C=O in Ar–COO–), 1612, 1508 (C–C in Ar), 1245, 1206 (C–O–C). ^1H NMR ($CDCl_3$, δ in ppm): 0.87–0.95 (m, CH_3), 1.11–2.37 (m, CH_2), 3.98 (m, OCH_2), 4.85 (m, COOCH), 5.44 (m, C=CH), 6.91 (m, Ar–H), 7.29 (m, Ar–H), 7.68 (m, Ar–H), 8.08 (m, Ar–H). Anal: calcd for $C_{78}H_{101}NO_{12}$, C 75.30, H 8.13, N 1.13; found C 74.11, H 7.69, N 1.54%.

2.4.7. *CP3*

CP3 was prepared by a procedure similar to that for **CP1**, using **M6** instead of **M5**. Yield: 56.0%. FTIR (KBr, ν_{max}/cm^{-1}): 2941, 2865 (CH_2), 2232 (CN), 1720 (C=O in Ar–COO–), 1611, 1509 (C–C in Ar), 1240, 1207 (C–O–C). ^1H NMR ($CDCl_3$, δ in ppm): 0.78–0.90 (m, CH_3), 1.11–2.09 (m, CH_2), 3.96 (m, CH_2O), 4.91 (m, COOCH), 6.89 (m, Ar–H), 7.25 (m, Ar–H), 7.63 (m, Ar–H), 8.04 (m, Ar–H). Anal: calcd for $C_{56}H_{65}NO_{12}$, C 71.26, H 6.89, N 1.48; found C 70.68, H 6.31, N 1.85%.

2.4.8. *CP4*

CP4 was prepared by a procedure similar to that for **CP2**, using **M6** instead of **M5**. Yield: 55.6%. FTIR (KBr, ν_{max}/cm^{-1}): 2938, 2869 (CH_2), 2227 (CN), 1722 (C=O in Ar–COO–), 1615, 1508 (C–C in Ar), 1245, 1206 (C–O–C). ^1H NMR ($CDCl_3$, δ in ppm): 0.87–1.05 (m, CH_3), 1.23–2.11 (m, CH_2), 3.99 (m, CH_2O), 4.95 (m, COOCH), 6.91 (m, Ar–H), 7.28 (m, Ar–H), 7.67 (m, Ar–H), 8.07 (m, Ar–H). Anal: calcd for $C_{61}H_{75}NO_{12}$, C 72.26, H 7.40, N 1.38; found C 72.45, H 7.24, N 2.01%.

2.4.9. *CP5*

CP5 was prepared by a procedure similar to that for **CP1**, using **M3** instead of **M1**. Yield: 51.0%. FTIR (KBr, ν_{max}/cm^{-1}): 2941, 2867 (CH_2), 1718 (C=O in Ar–COO–), 1608, 1512 (C–C in Ar), 1243, 1208 (C–O–C). ^1H NMR ($CDCl_3$, δ in ppm): 0.66–0.97 (m, CH_3), 1.06–2.29 (m, CH_2), 3.94–4.08 (m, CH_2O), 4.86 (m, COOCH), 5.42 (m, C=CH), 6.96 (m, Ar–H), 7.02 (m, Ar–H), 7.27 (m, Ar–H), 8.07 (m, Ar–H). Anal: calcd for $C_{76}H_{100}O_{13}$, C 74.75, H 8.20; found C 73.34, H 7.81%.

2.4.10. *CP6*

CP6 was prepared by a procedure similar to that for **CP1**, using **M4** instead of **M1**. Yield: 50.5%. FTIR (KBr, ν_{max}/cm^{-1}): 2944, 2870 (CH_2), 1723 (C=O in Ar–COO–), 1610, 1514 (C–C in Ar), 1245, 1209 (C–O–C). ^1H NMR ($CDCl_3$, δ in ppm): 0.70–0.98 (m, CH_3), 1.12–2.47 (m, CH_2), 3.96–4.27 (m, CH_2O), 4.78 (m, COOCH), 5.38 (m, C=CH), 6.91 (m, Ar–H), 7.07 (m, Ar–H), 7.27 (m, Ar–H), 8.09 (m, Ar–H). Anal: calcd for $C_{81}H_{110}O_{13}$, C 75.35, H 8.53; found C 74.11, H 8.38%.

2.4.11. *CP7*

CP7 was prepared by a procedure similar to that for **CP3**, using **M3** instead of **M1**. Yield: 62.0%. FTIR (KBr, ν_{max}/cm^{-1}): 2942, 2867 (CH_2), 1726 (C=O in Ar–COO–), 1609, 1512 (C–C in Ar), 1245, 1204 (C–O–C). ^1H NMR ($CDCl_3$, δ in ppm): 0.79–0.97 (m, CH_3), 1.12–2.40 (m, CH_2), 3.93 (m, CH_2O), 4.93 (m, COOCH), 6.88 (m, Ar–H), 7.04 (m, Ar–H), 7.27 (m, Ar–H), 8.31 (m, Ar–H). Anal: calcd for $C_{59}H_{74}O_{13}$, C 71.52, H 7.47; found C 71.25, H 7.397%.

2.4.12. *CP8*

CP8 was prepared by a procedure similar to that for **CP3**, using **M4** instead of **M1**. Yield: 45.0%. FTIR (KBr, ν_{max}/cm^{-1}): 2939, 2865 (CH_2), 1724 (C=O in Ar–COO–), 1612, 1516 (C–C in Ar), 1238, 1205 (C–O–C). ^1H NMR ($CDCl_3$, δ in ppm): 0.78–0.97 (m, CH_3), 1.16–2.35 (m, CH_2), 3.95 (m, CH_2O), 4.94 (m, COOCH), 6.90 (m, Ar–H), 7.05 (m, Ar–H), 7.27 (m, Ar–H), 8.08 (m, Ar–H). Anal: calcd for $C_{64}H_{84}O_{13}$, C 72.45, H 7.92; found C 72.74, H 8.11%.

2.5. Fabrication of liquid crystalline polymer films and cells

Glass plates were cleaned using a detergent solution, washed with water and then with acetone using ultrasonic equipment for 20 min and 60 min, respectively. After completion of the cleaning process, the plates were dried in vacuum. The polymer was heated to isotropic phase and then coated on a glass surface, cooled to liquid crystalline phase. The polymer was quenched and the optical properties of the liquid crystalline polymer films were then investigated. Furthermore, the liquid crystalline composite cells were fabricated by a pair of parallel pre-rubbed glass plates with a 15 μm gap. After filling the liquid crystal mixture, the glass cell was sealed with epoxy resin. The liquid crystal composite cells were prepared from a mixture of ZLI-2293 or E7/chiral dopant. Since ZLI-2293 is a nematic liquid crystal mixture, the composition is complex. For convenience, weight ratios of ZLI-2293 or E7/chiral dopant were used.

3. Results and discussion

3.1. Synthesis and characterization

A series of monomers with six and 11 methylene segment as spacer lengths, and electron releasing (–OR) and withdrawing (–CN) terminal groups were synthesized by the esterification of intermediate carboxylic acid monomer 4-(6-acryloyloxyhexyloxy) benzoic acid or 4-(6-acryloyloxyundecyloxy) benzoic acid and corresponding compounds with hydroxyl groups using DCC as the condensation agent and DMAP as the catalytic system in dry dichloromethane. The synthetic routes of the monomers are shown in Scheme 1. Elemental analysis, FTIR, ^1H, and ^{13}C NMR spectroscopic techniques were used to identify the structures and constitutional composition of target monomers, as shown in the Section 2. Cholesteryl and menthyl groups were attached at the end of chiral monomers **M5** and **M6**, respectively. The FTIR spectrum of **M6** showed characteristic bands at 2870–2934, 1704–1734, and 1505–1610 cm^{-1} attributable to the C–H, ester C=O, and aromatic C=C stretching bands, respectively. ^1H NMR spectrum of **M6** showed peaks at 6.96–8.16, 5.80–6.43, 4.90–4.97, and 4.00–4.20 ppm corresponding to aromatic, vinyl, C–H in menthyl group,

and –OCH_2 protons, respectively. A reasonable quantification of all protons of the synthesized monomers was also measured by peak area integrals in the ^{1}H NMR spectra. In order to investigate the induction of cholesteric liquid crystals, two chiral compounds **7** and **8** were also synthesized as shown in Scheme 2.

The free radical polymerization of the monomers initiated by AIBN in dry benzene makes the corresponding polymers with good yields. Homopolymerization and copolymerization of the synthesized monomers were carried out and the chemical structures of polymers are shown in Scheme 3. The chemical structures of homopolymers **P1**–**P4** and copolymers **CP1**–**CP8** were also confirmed by NMR spectrometry. The molecular weight and specific rotation of the polymers are summarized in Table 1. The occurrence of polymerization was proven by FTIR spectroscopy by checking the disappearance in the spectra of the absorption at around 1627–1636 cm^{-1} corresponding to the acrylic vinyl group. After polymerization, the corresponding signals of the vinyl group at 5.80–6.43 ppm disappeared completely, and the peaks of the chemical shifts of polymers were quite broad and consisted with the expected polymer structure. The final molar ratio composition of the copolymers incorporating chiral and liquid crystalline monomer as comonomer was assessed by ^{1}H NMR spectrometry by comparing the integrated signals in the aliphatic regions (menthyl or cholesteryl moiety) of chiral unit, located at 4.77–4.97 ppm, and in the aromatic regions of these two comonomers. The results are summarized in Table 1. The difference in the mesogenic core and the terminal groups of these monomers might affect both monomer interaction and polymerization rate leading to the variation of yields, final molar ratio and molecular weight of polymers. As shown in Table 1, the weight-average molecular weights (M_w) of **P1**–**P4** and **CP1**–**CP8**, determined by gel permeation chromatography against polystyrene as calibration standard, were in the range of 1.7×10^4–6.9×10^4, with polydispersity indices (PDI) lying around 1.40–2.45. The synthesized polymers are soluble in common organic solvents such as $CHCl_3$, THF, and toluene.

3.2. Liquid crystalline properties

The thermal properties and the phases of the synthesized monomers are summarized in Table 2. The phase sequence and phase transition temperatures of the synthesized monomers, obtained during the first cooling and the second heating cycles, are determined by DSC and summarized in Table 2. The data listed in Table 2 revealed that the effect of molecular structures on the melting temperature, mesomorphic properties, and even molecular arrangements of monomers was considerable. It indicates that the central and terminal units have high influences on the melting temperature, mesomorphic properties, and even molecular arrangements. In general, liquid crystals must contain suitable polarity and spacer length at the center and terminals. As seen from the data listed in Table 2, monomer **M3** with an electron releasing (–OC_4H_9) segment as terminal group exhibited monotropic mesophase and revealed nematic phase (N; schlieren texture) at the temperature range of 57.1–33.3 °C during cooling cycle. As compared to **M3**, **M4** with longer methylene segment as spacer lengths exhibited enantiotropic mesophase due to the increasing of polarity of monomer and molecular interaction. For monomer **M4**, during heating cycle, a melting transition, a smectic-to-nematic phase transition, and a nematic-to-isotropic phase transition appeared at 60.7, 63.3, and 64.3 °C, respectively, and an isotropic-to-nematic phase transition and crystallization temperature appeared during cooling cycle at 60.2 and 39.0 °C. **M4** revealed smectic phase due to the enhancement of the lateral molecular interaction of the side chains. As shown in Table 2, introduction of cholesteryl group in chiral monomer **M5** exhibited enantiotropic mesophase and revealed chiral nematic phase (N^*; oily streaks texture) during heating and cooling cycles. However, chiral monomer **M6** incorporating steric hindered menthyl group did not reveal any liquid crystalline phases. The result suggests that steric hindered menthyl group might decrease the molecular interaction between molecules leading to the absence of liquid crystalline phases. The liquid crystalline phases were confirmed by DSC and X-ray diffraction analyses and were also compared with the polarized optical

Table 2
Phase transition temperature[a] (°C) and specific rotation of monomers and chiral dopants

Compounds	Phase transition temperature (°C), enthalpy change (J/g)		$[\alpha]_D$[c] (°)
	Heating cycle[b]	Cooling cycle[b]	
M1	K 78.0 N I, 104.2	I 57.4 K, −86.5	–
M2	K 85.2 I, 120.5	I 66.7 K, −80.1	–
M3	K 62.8 I, 48.1	I 57.1 N 33.3 K, −1.5, −32.5	–
M4	K 60.7 S_A 63.3 N 64.3 I, 75.2, 8.5, 2.8	I 60.2 N 39.0 K, −5.9, −56.2	–
M5	K 130.2 N^* 205.4 I, 52.5, 0.5	I 198.5 N^* 102.6 K, −0.6, −20.4	−12.5
M6	K 32.6 I, 25.4	I 12.5 K, −7.9	−46.2
7	K 116.3 I, 54.2	I 46.1 K, −37.8	−65.0
8	K 141.8 I, 41.0	I 63.0 K, −38.9	−64.2

[a] Enthalpy of the phase change during second heating and first cooling at a rate of 10 K min^{-1}.
[b] K, crystal; N, nematic; S_A, smectic A; N^*, chiral nematic; I, isotropic phase.
[c] Specific rotation of compounds, 0.1 g in 10 ml $CHCl_3$.

Table 1
Results of polymerization[a]

No.	Phase transition temperature[b] (°C)		Composition		M_w[d] ($\times 10^4$)	PDI[d]	$[\alpha]_D$[e] (°)
	Heating cycle	Cooling cycle	Comonomer	x/y[c]			
P1	G 32.0 N 125.4 I	I 122.8 N 31.8 G	**M1**	–	3.1	2.31	–
P2	G 57.2 S_C 78.3 S_A 156.8 I	I 151.3 S_A 57.5 S_C 36.3 G	**M2**	–	2.4	2.17	–
P3	G 57.8 S_A 113.8 N 123.5 I	I 122.0 S_A 108.7 N 35.8 G	**M3**	–	6.9	1.95	–
P4	G 77.3 S_A 136.0 I	I 131.5 S_A 71.6 G	**M4**	–	5.9	1.98	–
CP1	G 38.0 S_A^* 110.5 I	I 116.0 S_A^* 36.1 G	**M1**/**M5**	72.2/27.8	3.0	2.45	−1.4
CP2	G 46.2 S_A^* 140.8 I	I 137.6 S_A^* 39.4 G	**M2**/**M5**	75.4/24.6	2.1	2.37	−1.1
CP3	G 35.9 S_A^* 163.2 I	I 157.6 S_A^*35.8 G	**M1**/**M6**	80.3/19.7	3.3	1.94	−9.6
CP4	G 32.9 S_A^* 139.4 I	I 134.6 S_A^* 31.8 G	**M2**/**M6**	81.5/18.5	2.2	2.05	−6.2
CP5	G 68.5 S_A^* 161.7 I	I 160.1 S_A^* 74.3 G	**M3**/**M5**	72.3/27.7	4.2	2.32	−2.8
CP6	G 45.5 S_A^* 152.4 I	I 152.0 S_A^* 43.8 G	**M4**/**M5**	78.6/21.4	3.0	2.44	−1.2
CP7	G 21.3 S_A^* 87.0 I	I 85.6 S_A^* 20.8 G	**M3**/**M6**	73.0/27.0	5.2	1.40	−9.2
CP8	G 58.7 S_A^* 107.0 I	I 106.5 S_A^* 51.8 G	**M4**/**M6**	79.8/20.2	1.7	1.82	−4.1

[a] In benzene at 60 °C for 24 h in the presence of 3 mol% AIBN; feed molar ratio $x/y = 83/17$ for copolymers **CP1**–**CP8**.
[b] G, glassy; N, nematic; S_A, smectic A; S_C, smectic C; S_A^*, chiral smectic A; I, isotropic phase.
[c] Final molar ratio, estimated by ^{1}H NMR spectroscopy.
[d] M_w, and PDI of the polymers were determined by gel permeation chromatography using polystyrene standards and $CHCl_3$ as eluent.
[e] Specific rotation of compounds, 0.1 g in 10 ml $CHCl_3$.

microscopic (POM) textures reported in the literature [23]. The POM textures of the monomers **M4** and **M5** are shown in Fig. 1. Both chiral compounds **7** and **8** revealed no mesophases. Similar to regular liquid crystals, rearrangement of compounds **7** and **8** need a certain period of time and appear at different lower phase transition temperature degree.

As shown in Scheme 3, rod-like molecules of the monomers with high polar hindered pendant groups were observed. Also, as seen in Table 1, all synthesized polymers revealed to have high interaction between side chain units leading to the generation of mesophases. As shown in Table 1 and Scheme 3, achiral homopolymer **P1** containing withdrawing (–CN) terminal group exhibited nematic characteristic, however, **P2** with longer methylene segment as spacer lengths revealed smectic A (fan-shape texture) and smectic C phases (striated fan-shape texture). It suggests that the formation of the tilted smectic phase (S_C) might due to the existence of terminal polar (–CN) structure in molecules [24]. Contrary to that, **P3** containing releasing ($-OC_4H_9$) terminal group revealed nematic (schlieren texture) and smectic A (fan-shape texture) phases. As compared with **P3**, **P4** containing longer methylene unit in side chain only exhibited smectic A phase. The results indicate that the variation in spacer length might affect both the freedom of the mesogenic unit from the polymer backbone and the aspect ratio of the side chain unit. This also indicates that the terminal substituent is important in size and in the nature of its polarity. Consequently, the intermolecular interaction, dipole-induced dipole interactions might play an important role in determining the type of mesophase textures and influence the physical properties of the polymers [25]. All copolymers incorporating chiral monomer **M5** or **M6** with cholesteryl or menthyl group as terminal group revealed chiral smectic A phases (fan-shape texture). As shown in Scheme 3, **CP1**–**CP2** and **CP5**–**CP6** with cholesteryl segment as terminal groups exhibited chiral smectic A phases. However, the expected chiral nematic (cholesteric) phases were not observed. The results suggest that the polymer chains might hinder the formation of a helical supermolecular mesogenic structure and the mesogenic moieties are ordered in a smectic orientation [26,27]. Fig. 2 shows the DSC thermograms of **P4** and **CP8** at a heating rate of 10 K min^{-1}. The phase transition temperatures and the enthalpy of the polymers were also estimated. Fig. 3 shows the crossed POM textures of **P2**, **P3** and **CP8**.

Depending on the molecular structures, chirality and the ligands around the chiral center, optical right and left rotations of the compounds were observed. The (*R*)- or (*S*)- chiral configuration in mesophases changes or induces, for example, the size of pitch of the cholesteric (N^*) and smectic phases (e.g. S_C^*), or leads to other chiral structures by short or long range orientational order. In principle, specific rotation reveals the characteristic of net vector of the polarity of the chiral molecules on plane polarized light. The specific rotation was evaluated at 30 °C in chloroform using a Jasco DIP-370 polarimeter with the D-line of sodium ($\lambda = 589$ nm) reading to $\pm 0.001°$. The specific rotation of cholesterol and menthol are $-36°$ and $-51°$, respectively. Accordingly, the specific rotation of the chiral monomers revealed negative values. As can be seen in Table 2, monomer **M6** end capped with menthyl group revealed higher specific rotation than that of monomer **M5** with cholesteryl group. Both chiral compounds **7** and **8** revealed high negative

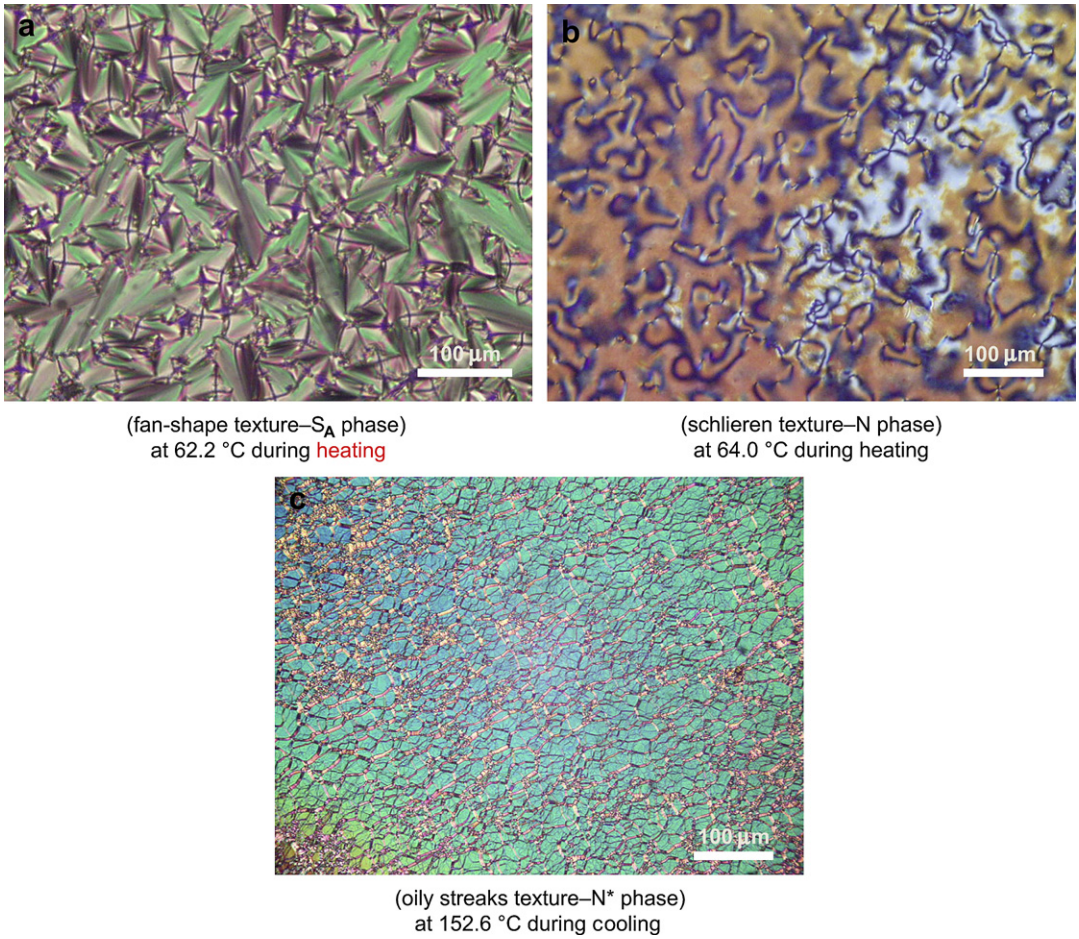

(fan-shape texture–S_A phase) at 62.2 °C during heating

(schlieren texture–N phase) at 64.0 °C during heating

(oily streaks texture–N* phase) at 152.6 °C during cooling

Fig. 1. Polarizing microscopic textures of compounds: (a), (b) **M4**, and (c) **M5** (100× magnification).

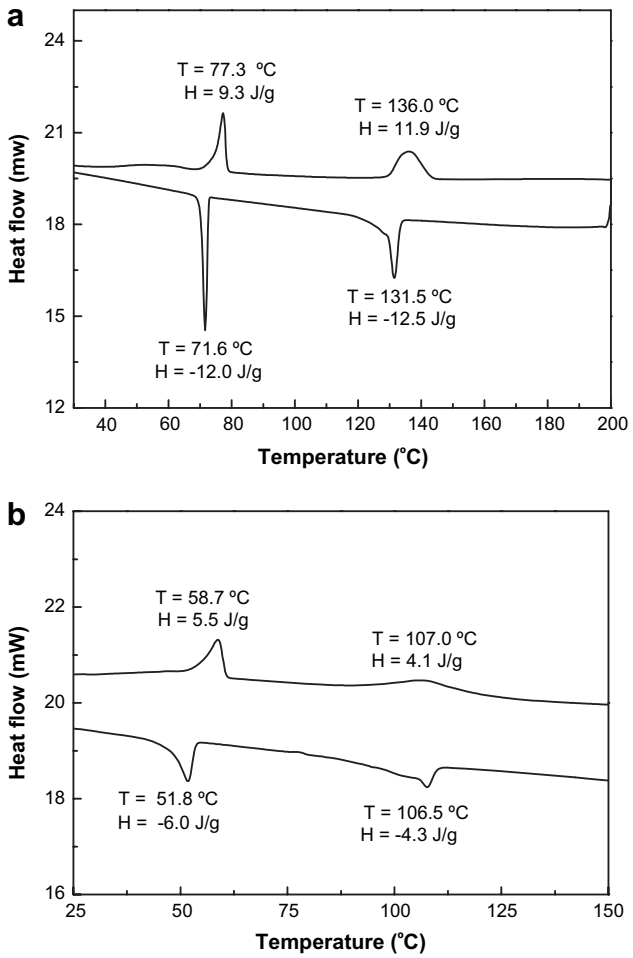

Fig. 2. DSC thermograms of polymers: (a) **P4** and (b) **CP8** at a heating rate of 10 K min^{-1}.

specific rotation values. This maybe due to the steric hindrance of the terminal groups leading to the generation of high specific rotation values. The specific rotation of the copolymers was also estimated. Specifically, it was found that chirality could be a factor, which affects the physical properties of the polymers. Cleavage of the double bond and the binding of other monomers together did not seem to significantly affect the chirality of the compounds. The results indicate that the specific rotation was influenced by the coherence of polarity due to chemical bonding after polymerization. In principle, copolymers contain only a few parts of the chiral unit. Accordingly, the specific rotation of the copolymers is lower than that of the chiral monomers and the chiral homopolymers.

3.3. Thermal stability of polymers

Thermal stability of the polymers was also studied using TGA under nitrogen atmosphere and the results are summarized in Table 3. Polymers revealed high thermal stability with decomposition temperatures (T_d) at 10% weight loss greater than 384 °C and about 50% weight loss occurred beyond 442 °C under nitrogen atmosphere. The results suggest that the existence of the longer mesogenic side chain might cause a strong interaction between the repeating units leading to the increase of thermal resistance. Degradation of 10% weight loss around (384–423 °C) and the thermal decomposition occurred around 500 °C could be considered as the thermal cleavage of carbonyl groups or the scission of other C–O bonds in side chains and the decomposition of polymer backbone in copolymers, respectively [28].

3.4. X-ray diffraction of polymers

To further elucidate the structures of the mesophases, X-ray diffraction measurements of polymers were carried out. X-ray diffraction is a powerful analytical tool to determine the crystal structure, orientation and sequence distribution of polymers [29]. Samples were heated to the temperature ranges of the mesophases and then quenched. Fig. 4(a) and (b) shows the X-ray diffraction curves of the homopolymer **P1** and copolymer **CP8**, respectively. The X-ray diffraction curve of the homopolymer **P1** showed a typical nematic characteristic of broad peak at around $2\theta = 20$–25°, classically due to average intermolecular spacings of approximately 3–5 Å at mesophases and no peak appeared in the small angle region. The X-ray pattern of the copolymer **CP8** showed a sharp and strong peak at a small angle region around $2\theta = 3.18^\circ$, corresponding to the layer *d*-spacing value of 27.7 Å at 90.5 °C under cooling, and a broad peak in the wide angle region associated with lateral packings in the range of $2\theta = 20$–30°, implying a smectic structure of the polymer. Furthermore, a fan-shaped texture could be clearly observed by POM, as shown in Fig. 3(d), which is a characteristic texture of the smectic A phase. According to the molecular modeling calculation using CS Chem3DPro, employing MM2 energy parameters, the estimated all-*trans* molecular length *l* of the most extended conformation of chiral monomer **M4** is around 29.2 Å (the layer *d*-spacing value is ca. 27.7 Å by XRD patterns; $d/l = 0.95$). Therefore, a possible layer structure of **CP8** is suggested to exhibit monolayer packing of the side chains [30].

3.5. Induction of cholesteric liquid crystals

Chiral dopant **7** containing photoisomerizable cinnamoyl groups in the *E* form shows maximum absorption at around 280 nm in $CHCl_3$ solution which is attributed to the π–π^* transition of the *E*-form isomers. UV irradiation caused a decrease in absorption band with an increase in UV ($\lambda_{irr} = 300$ nm) irradiation time period. The decrease was induced by the *E*–*Z* configurational isomerization at the C=C segments. Fig. 5(a) shows the variation of UV–vis spectra of the chiral dopant **7** during UV ($\lambda_{irr} = 300$ nm) irradiation time period. Fig. 5(b) shows the thermal stability of the *Z* form isomer. After UV irradiation, the sample was given heat treatment at 50 °C for certain minutes. The results in Fig. 5(b) suggest that photo-induced *Z* form configurational isomer is thermally stable. The thermal stability of the chiral dopant **7** was further confirmed by polarimeter. The specific rotation of the sample solution was measured at various temperatures as shown in Fig. 6. No significant change could be seen during the variation of the temperatures. The results suggest that heat treatment could not cause the configurational isomerization of the chiral compound **7**.

Due to the presence of the molecular chirality, the cholesterically ordered material has regions, which selectively reflect circularly polarized electromagnetic radiation of a band of wavelengths. The central wavelength (λ_0) of the band of reflected wavelengths is determined by the pitch (p) of the molecular helix, according to the following formula

$$\lambda_0 = \bar{n} p \cos\theta \quad (1)$$

where $\bar{n}$ is the average refractive index of the cholesterically ordered material and θ is the angle of incidence of the beam. The bandwidth $\Delta\lambda$ is given by

$$\Delta\lambda = p \times \Delta n \quad (2)$$

where Δn is the birefringence of the uniaxially oriented phase corresponding to the cholesterically ordered phase. In the visible range, the regions selectively reflect circularly polarized light of a particular color [31,32]. The influence of the copolymer

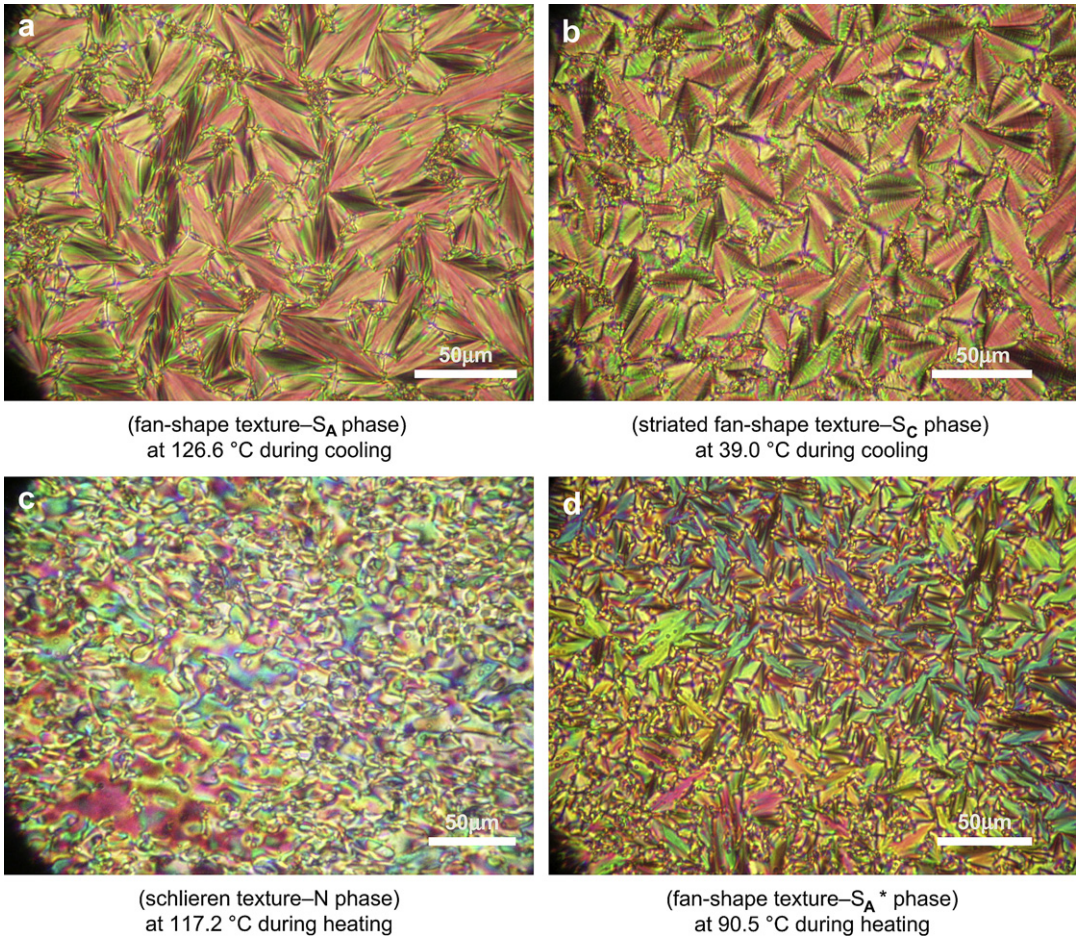

Fig. 3. Polarizing microscopic textures of polymers: (a), (b) **P2**, (c) **P3**, and (d) **CP8** (400× magnification).

composition on the pitch of the cholesteric helix and therewith the reflection wavelength is described by the helical twisting power (HTP) which is defined as the initial slope of the inverse helical pitch p^{-1} vs. the mole fraction x of the chiral dopant [10].

$$\mathrm{HTP} = \left(\frac{\mathrm{d}p^{-1}}{\mathrm{d}x}\right)_T = \bar{n}\left(\frac{\mathrm{d}\lambda_0^{-1}}{\mathrm{d}x}\right)_T \tag{3}$$

In order to ensure the stability of the induction of chiral dopants on the liquid crystals, commercially available nematic liquid crystalline mixture ZLI-2293 or E7 was used as host liquid crystal. Synthesized chiral compounds **7** and **8** were added to the host as a chiral dopant. The optical properties of the induced cholesteric liquid crystalline phases are summarized in Table 4. Typical reflection band of cholesteric liquid crystalline cells was obtained and optical properties are summarized in Table 4. From the results of the reflection band of cholesteric cells, chiral dopant **7** revealed a higher helical twisting power (HTP) than chiral dopant **8**. The helical twisting power depends on molecular interactions between molecules of chiral compounds (solute) and host liquid crystals (solvent) [33,34]. Higher concentration of dopant **7** caused a blue shift as shown in entries 2 and 4 of Table 4 and Fig. 7. Chiral dopant **8** showed weaker HTP value as shown in entries 5 and 6. Fig. 7 shows the concentration effect of dopant **7** on the reflection band of the fabricated liquid crystal cells. An increase of chiral dopant concentration caused blue shifts, which were shifted from the infrared to a visible light region and the bandwidth of the reflected light peak was narrowed.

Photo-induced *E–Z* isomerization of chiral dopant 7 could change the cholesteric pitch leading to the variation of the reflection color of the cells. Fig. 8(a) shows the dependence of UV irradiation on the reflection band of cholesteric cell with the ratio of ZLI-2293:**7** = 10:2. Fig. 8(b)–(d) shows the real appearances of the recorded color pattern. Depending on UV irradiation time, the colors of the exposed areas were found to be different. The color patterns of R/G/B could be obtained through various masks as shown in Fig. 8(b) and (d).

Table 3
Thermal stability of polymers[a]

Polymer	10% Weight loss temperature (°C)	50% Weight loss temperature (°C)	Residue at 600 °C (wt%)
P1	410.2	455.1	6.98
P2	414.1	455.3	3.77
P3	423.6	466.5	1.24
P4	422.1	458.9	1.18
CP1	386.7	442.8	5.53
CP2	390.5	447.2	4.46
CP3	388.2	458.9	5.27
CP4	392.5	457.4	4.04
CP5	384.0	442.5	5.14
CP6	391.3	445.3	3.96
CP7	407.8	466.8	4.53
CP8	410.8	455.3	1.17

[a] Estimated using TGA at a heating rate of 40 K min^{-1}.

3.6. Fabrication and characterization of polymer films

As shown in Table 1, all synthesized polymers revealed chiral smectic A phases. In order to fabricate the cholesteric liquid

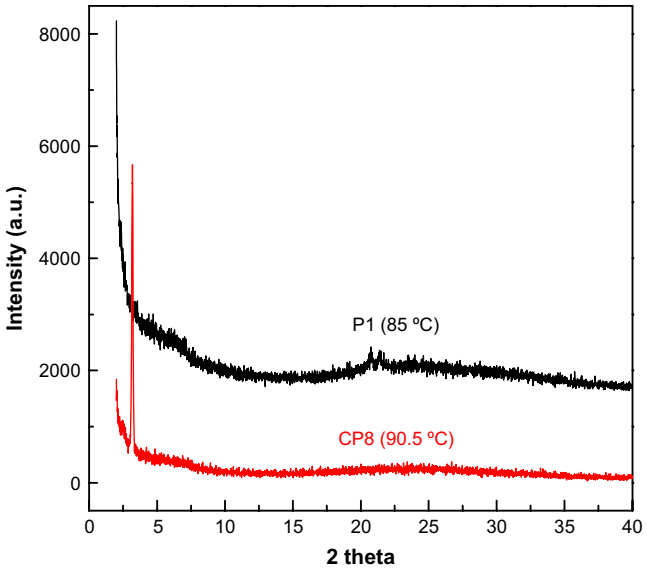

Fig. 4. X-ray diffraction curves of polymers: (a) **P1** and (b) **CP8**.

crystalline films, chiral dopants **7** and **8** were added into the polymer materials. The physical properties of the induced cholesteric liquid crystalline films are summarized in Table 5. Films F1 to F6 containing **P4** as host materials with various quantities of chiral

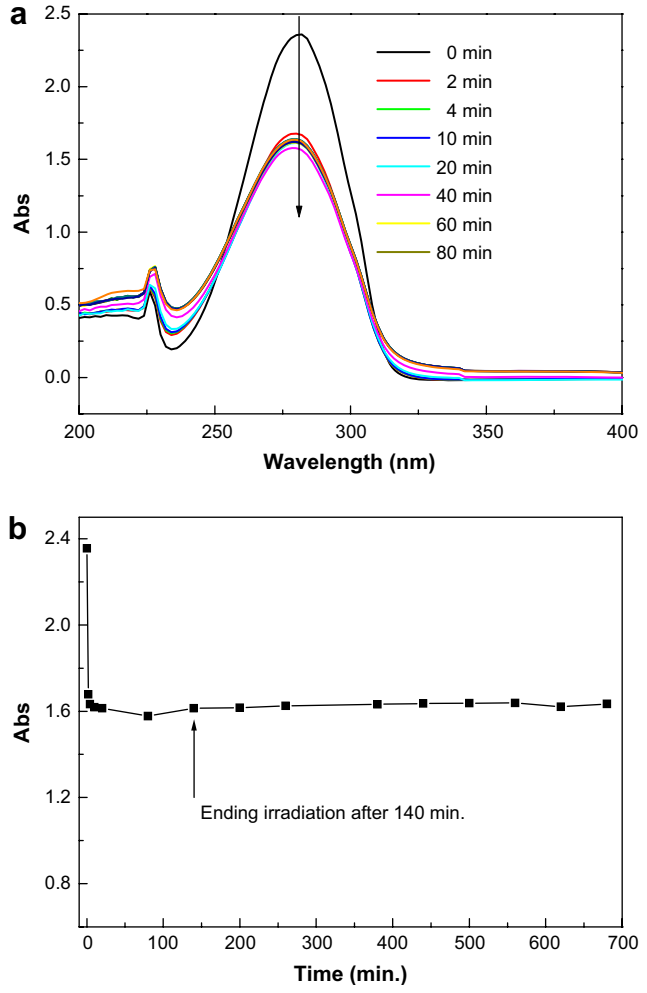

Fig. 5. (a) UV–vis spectra of compound **7** and (b) variations of the maximum absorption at λ_{280} before and after UV irradiation.

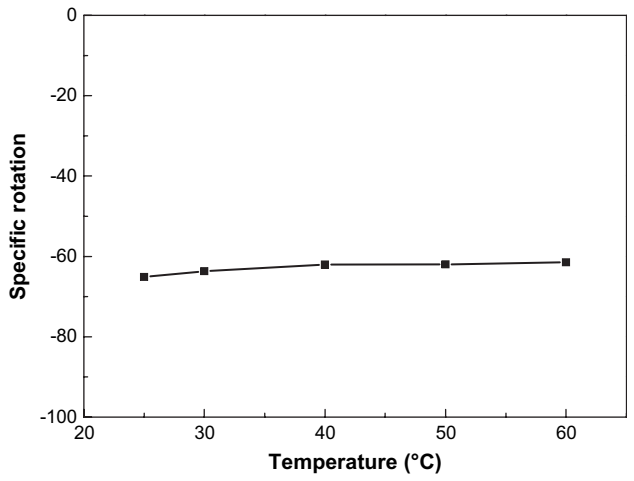

Fig. 6. Dependence of specific rotation ($[\alpha]_D$) of compound **7** on temperature.

dopant **7** or **8** revealed chiral smectic A phases. The results suggest that the blending of chiral dopant in **P4** might influence the packings of polymer chain, leading to the variation of smectic A (S_A) to chiral smectic mesophases (S_A^*). Contrary to that, the introduction of chiral dopant **7** or **8** into **CP6** (S_A^*) might disturb the molecular orientation of side chains and decrease the lateral molecular interaction, leading to the variation of chiral smectic A (S_A^*) to chiral nematic mesophases (N^*), and a decrease in the range of phase transition temperatures. It also indicates that further addition of the chiral dopants **7** and **8** increases the twisting driving forces leading to the formation of the chiral nematic phases of both F7 and

Table 4
Effects of chiral dopants on reflected band of cholesteric cells with various nematic LC

Entry	Nematic LC	Chiral dopant	Weight ratio	λ_0[a] (nm)	$\Delta\lambda$[b] (nm)	HTP[c] (μm^{-1})
1	ZLI-2293	**7**	10:1	640	40	26.9
2	ZLI-2293	**7**	10:1.5	515	35	23.3
3	E7	**7**	10:1	662	65	26.0
4	E7	**7**	10:1.5	530	60	24.6
5	ZLI-2293	**8**	10:1.5	660	80	18.2
6	E7	**8**	10:1.5	875	40	14.3

[a] Central wavelength of reflection.
[b] Reflective bandwidth.
[c] Helical twisting power.

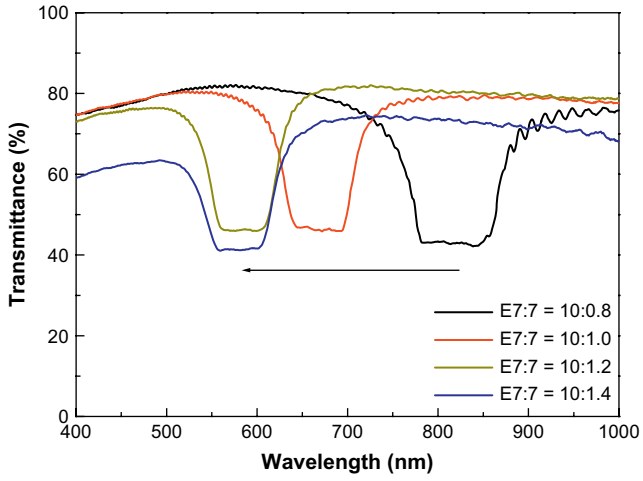

Fig. 7. Concentration effect of compound **7** on the reflected band of cholesteric liquid crystal cells.

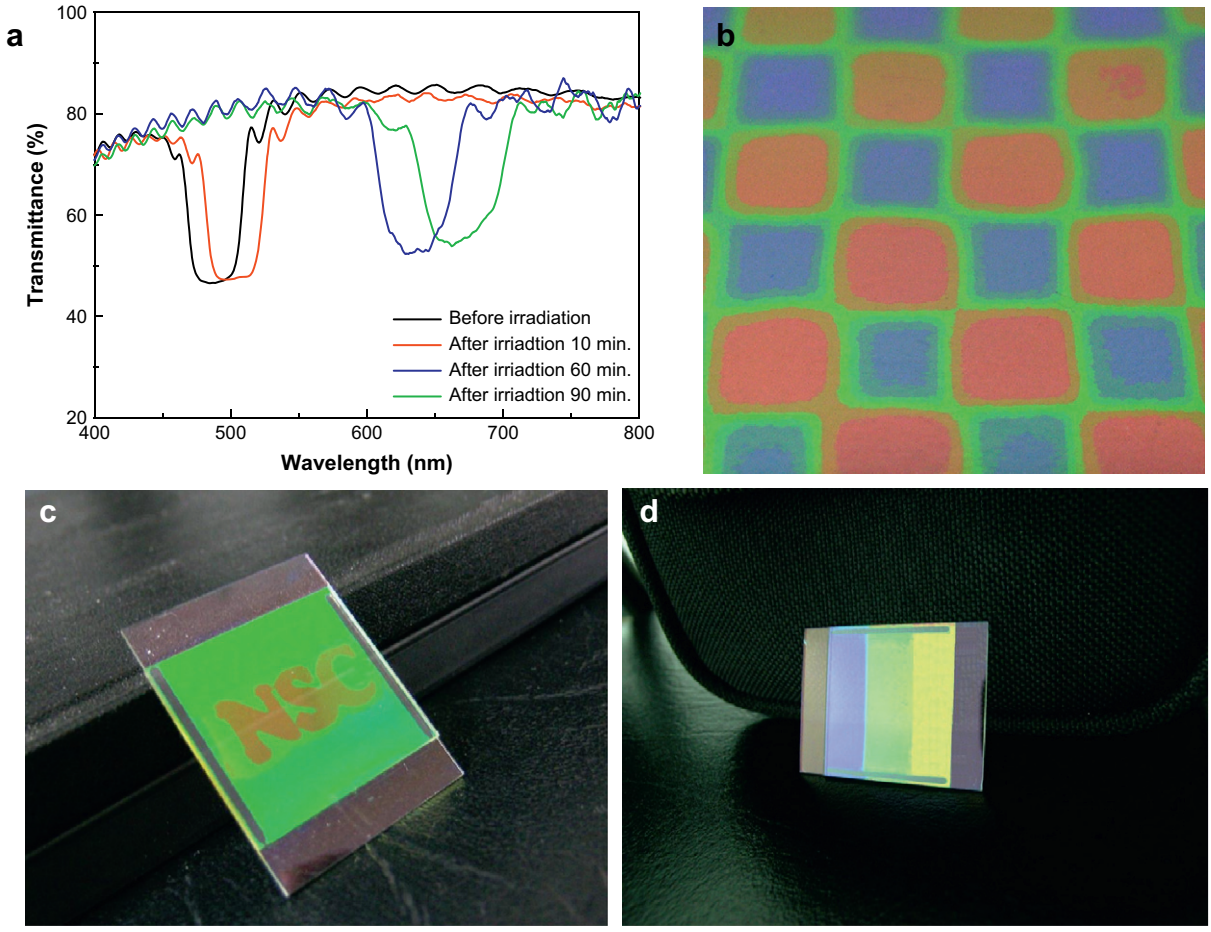

Fig. 8. (a) Effect of UV irradiation on cholesteric liquid crystal cells; UV exposure of cholesteric liquid crystal cells through masks with (b) chequer pattern, (c) words, and (d) grayscale (ZLI-2293:**7** = 10:2).

F8. Fig. 9 shows DSC thermograms of the polymer film F7. The planar textures with oily streaks were further confirmed by POM textures. Typical colorful reflection of the cholesteric polymer films is shown in Fig. 10(a). The helical morphology of cholesteric liquid crystalline film F8 is demonstrated in Fig. 10(b). The pitch length (about 560 nm) of cholesteric liquid crystalline film F8 was estimated. It indicates that the helical pitch and the reflection band of the cholesteric phase depend chiefly on the polymer structure such as the polymer backbone, the rigidity of the mesogenic core, the flexible spacer length, the polymer composition, and external forces.

Table 5
Phase transition temperatures of composite polymers

Polymer films[a]	Chiral dopant[b] (wt%)	Heating cycle[c] (°C)	Cooling cycle[c] (°C)
P4[d]	0	G 77.3 S_A 136.0 I	I 131.5 S_A 71.6 G
F1	**7** (5)	G 74.7 S_A^* 117.5 I	I 108.5 S_A^* 67.4 G
F2	**7** (10)	G 75.4 S_A^* 118.2 I	I 109.5 S_A^* 68.0 G
F3	**7** (20)	G 75.5 S_A^* 110.5 I	I 96.3 S_A^* 68.1 G
F4	**8** (5)	G 77.5 S_A^* 132.3 I	I 125.6 S_A^* 64.8 G
F5	**8** (10)	G 76.5 S_A^* 131.3 I	I 121.9 S_A^* 63.1 G
F6	**8** (20)	G 72.0 S_A^* 119.5 I	I 107.9 S_A^* 63.9 G
CP6[d]	0	G 45.5 S_A^* 152.4 I	I 152.0 S_A^* 43.8 G
F7	**7** (20)	G 75.1 N^* 118.2 I	I 110.4 N^* 68.2 G
F8	**8** (20)	G 76.3 N^* 131.0 I	I 122.2 N^* 62.9 G

[a] Polymer films consist of achiral homopolymer **P4**/chiral copolymer **CP6** and chiral dopant **7** or **8**.
[b] Added chiral dopant **7** or **8** in weight percent.
[c] G, glassy; S_A, smectic A; N^*, chiral nematic; S_A^*, chiral smectic A; I, isotropic phase.
[d] **P4**, achiral homopolymer; **CP6**, chiral copolymer; without any addition of chiral dopant.

The undulated textures in the helical structure might be due to the unsophisticated process of cutting and thermal annealing treatments. These UV inducible photochromic polymer films are expected to be useful in the field of colorful image recording materials.

4. Conclusions

A series of new chiral monomers and polymers were synthesized. All chiral copolymers revealed chiral smectic A phases.

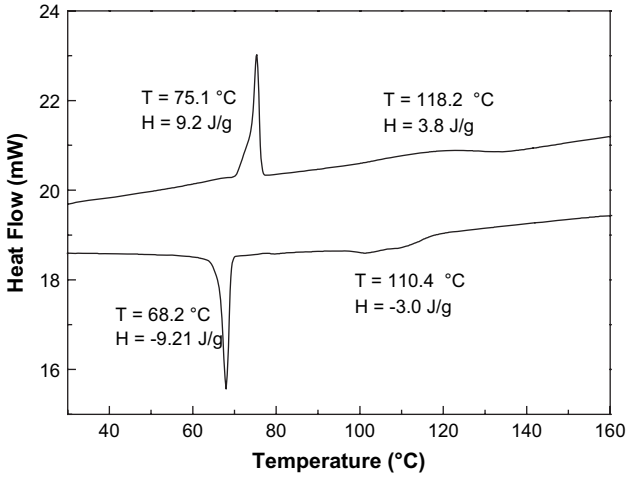

Fig. 9. DSC thermograms of polymer film F7 at a heating rate of 10 K min^{-1}.

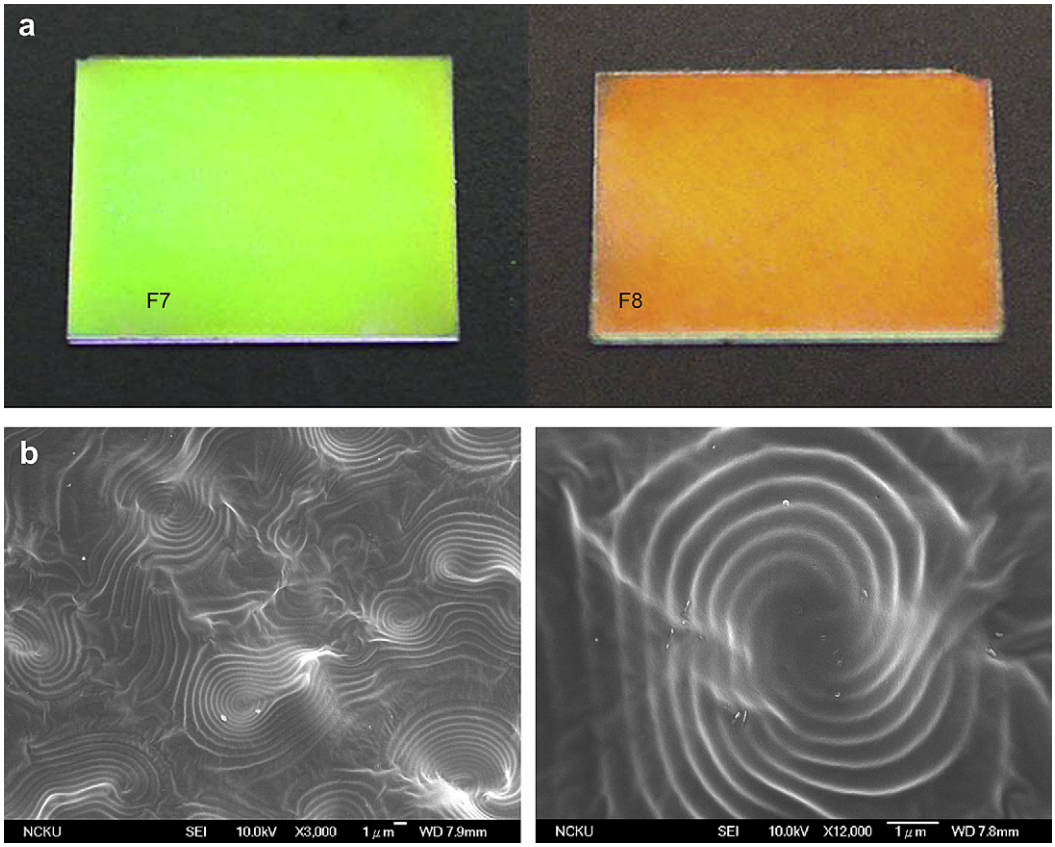

Fig. 10. (a) Appearances of the polymer films F7 and F8, and (b) SEM microphotographs of polymer film F8 at different magnifications.

Further addition of both synthesized chiral dopants **7** and **8** into chiral copolymer **CP6** induced chiral nematic N^* phases. Photo-induced *E*/*Z* isomerization of chiral dopant **7** changed the cholesteric pitch leading to the variation of the reflection color of the cells. Liquid crystalline polymers synthesized in this investigation revealing chiral nematic phases are expected to have a high potential for the preparation of image recordable films.

Acknowledgements

The authors would like to thank the National Science Council of the Republic of China (Taiwan) for financially supporting this research under contract no. NSC 96-2221-E-006-009.

Appendix. Supplementary data

Supplementary data associated with this article can be found in the online version, at doi:10.1016/j.polymer.2008.07.009.

References

[1] (a) Finkelmann H, Ringsdorf H, Wendorff JH. Makromol Chem 1978;179:273; (b) Ichimura K. Chem Rev 2000;100:1847.
[2] Zhao Y, Yuan G, Roche P. Polymer 1999;40:3025.
[3] Nair BR, Gregoriou VG, Hammond PT. Polymer 2000;41:2961.
[4] Suzuki K, Saito H, Tokita M, Watanabe J. Polymer 2005;46:8313.
[5] Bobrovsky AY, Boiko NI, Shibaev VP, Springer J. Adv Mater 2000;12:1180.
[6] Meyer JG, Ruhmann R, Sumpe J. Macromolecules 2000;33:843.
[7] Bobrovsky A, Shibaev V. Polymer 2006;47:4310.
[8] Giménez R, Millaruelo M, Piñol M, Serrano JL, Viñuales A, Rosenhauer R, et al. Polymer 2005;46:9230.
[9] Ruslim C, Ichimura K. J Mater Chem 2002;12:3377.
[10] Shibaev VP, Bobrovsky AY, Boiko NI. Prog Polym Sci 2003;28:729.
[11] Sackman E, Meiboom S, Snyder LC, Meixner AE, Dietz RE. J Am Chem Soc 1968; 90:3567.
[12] Lee HK, Doi K, Harada H, Tsutsumi O, Kanazawa A, Shiono T, et al. J Phys Chem B 2000;104:7023.
[13] Ruslim C, Ichimura K. J Phys Chem B 2000;104:6529.
[14] Yoshioka T, Ogata T, Zahangir AM, Nonaka T, Kurihara S. Liq Cryst 2004;31:15.
[15] Liu JH, Hsieh CD, Wang HY. J Polym Sci Part A Polym Chem 2004;42:1075.
[16] Lin TH, Chen YJ, Wu CH, Fuh YG, Liu JH, Yang PC. Appl Phys Lett 2005;86: 161120.
[17] Liu JH, Yang PC. Polymer 2006;47:4925.
[18] Liu JH, Hung HJ, Yang PC, Tien KH. J Polym Sci Part A Polym Chem, in press.
[19] Liu JH, Yang PC, Chiu YH, Suda Y. J Polym Sci Part A Polym Chem 2007;45:2026.
[20] Yang PC, Liu JH. J Polym Sci Part A Polym Chem 2008;46:1289.
[21] Yang PC, Wu MZ, Liu JH. Polymer 2008;49:2845.
[22] Portugall M, Ringsdorf H, Zentel R. Makromol Chem 1982;183:2311.
[23] (a) Dierking I. Textures of liquid crystals. Weinheim: Wiley-VCH; 2003; (b) Hans K, Rolf H. Handbook of liquid crystals. Weinheim: Verlag Chemie; 1980; (c) http://bly.colorado.edu/lcphysics/textures/.
[24] Collings PJ, Hird M. Introduction to liquid crystals chemistry and physics. London: Taylor and Francis; 1997 [chapter 3].
[25] Rameshbabu K, Kannan P, Velu R, Ramamurthy P. Liq Cryst 2005;32:823.
[26] Zhang BY, Hu JS, Jia YG, Du BG. Macromol Chem Phys 2003;204:2123.
[27] Zhang BY, Meng FB, Li QY, Tian M. Langmuir 2007;23:6385.
[28] (a) Li XG, Huang MR. Polym Degrad Stab 1999;64:81; (b) Huang MR, Li XG. J Appl Polym Sci 1998;68:293.
[29] Li XG, Huang MR. Angew Makromol Chem 1997;249:93.
[30] (a) McArdle CB. Side chain liquid crystal polymers. New York, NY: Blackie; 1989 [chapter 6]; (b) Hu JS, Zhang BY, Zhou AJ, Yang LQ, Wang B. Eur Polym J 2006;42:2849.
[31] Brehmer M, Lub J, Van de witte P. Adv Mater 1998;10:1438–41.
[32] Demus D, Goodby J, Grey G, Spiess H, Vill V, editors. Handbook of liquid crystals. New York: Wiley; 1998.
[33] Baessler H, Labes MM. J Chem Phys 1970;52:631.
[34] Celebre G, Luca GD, Maiorino M, Iemma F, Ferrarini A, Pieraccini S, et al. J Am Chem Soc 2005;127:11736.